RESEARCH ARTICLE

Check for updates

Exposing coordination-unsaturated Co sites in Co-MOF for efficient photocatalytic water oxidation†

Jie-Yi Zhou,[a] Xin-Yu Guan,[a] Hui-Ping Zhang,[a] Dong Luo,*[a] Xusheng Wang, [ID] *[b,c] Xiao-Ping Zhou [ID] *[a] and Dan Li [ID] [a]

Water oxidation to molecular dioxygen driven by visible light is essential but difficult in solar fuel production due to its sluggish reaction kinetics. Although the catalytic process is highly dependent on the coordination-unsaturated metal sites in coordination catalysts, the controllable design of catalysts with such catalytic sites remains challenging. Herein, we report two new Co-MOFs (**CoBIM-1** and **CoBIM-2**) for photocatalytic water oxidation under visible light. The coordination environment of Co in Co-MOFs can be easily manipulated by changing the atmosphere and concentration of deprotonated solvent during synthesis. **CoBIM-1** with coordinatively unsaturated Co sites showed good performance with an O_2 production of 2.0 mmol g^{-1} h^{-1}, in sharp contrast to its counterpart **CoBIM-2**. Furthermore, through isotope tracing experiments, we confirmed that the dioxygen was produced from water oxidation. This work highlights that the atmosphere during synthesis and solvent selection greatly regulate the crystal structures of MOFs and further manipulate their photocatalytic performance.

Introduction

With the depletion of fossil fuels and increasing environmental problems, it is urgent to look for clean and renewable energy sources that can replace traditional fossil energy. Photosynthesis in nature is the process by which green plants convert carbon dioxide and water into food using energy obtained from sunlight. Fortunately, mimicking natural photosynthesis in plants, artificial photosynthesis, a promising strategy for storing solar energy, is being explored to produce solar fuel.[1–3] In both natural and artificial photosynthesis, the water oxidation half-reaction is essential and more challenging compared to the reductive ones. It requires the transfer of 4e⁻ and 4H⁺ with the concomitant formation of an O=O bond, leading to high energy barriers and slow kinetics in addition to uphill reaction thermodynamics.[4] In natural photosynthesis, the

[a] College of Chemistry and Materials Science, Guangdong Provincial Key Laboratory of Supramolecular Coordination Chemistry, Jinan University, Guangzhou 510632, P. R. China. E-mail: luodong@jnu.edu.cn, zhouxp@jnu.edu.cn
[b] Institute of Functional Porous Materials, School of Materials Science and Engineering, Zhejiang Sci-Tech University, Hangzhou 310018, P. R. China. E-mail: xswang@zstu.edu.cn
[c] Key Laboratory of Green Cleaning Technology & Detergent of Zhejiang Province, Lishui, Zhejiang, 323000, P. R. China
†Electronic supplementary information (ESI) available. CCDC 2203264 and 2204131. For ESI and crystallographic data in CIF or other electronic format see DOI: https://doi.org/10.1039/d4qi00968a

heart of the photosystem II with an active Mn_4CaO_5 core is responsible for biocatalytic water oxidation, and the accessible metal sites in this active Mn_4CaO_5 center are regarded as active sites.[5–7] To mimic natural photosynthesis, precious metal oxides such as IrO_2 and RuO_2 have been proven to be the most effective water oxidation catalysts (WOCs), but catalysts with low-cost elements are more attractive.[8–10] Recently, cobalt-based catalysts have shown potential as WOCs, such as Co_3O_4, $Co(PO_3)_2$, $Li_2Co_2O_4$, Co-polyoxometalate, Co-based metal–organic cages, *etc.*[11–15] Due to the lack of porosity of these photocatalysts, typically only surface cobalt sites can be utilized to catalyse water oxidation reactions, thereby limiting their catalytic efficiency.

Metal–organic frameworks (MOFs) composed of metal ions or clusters and polytopic organic linkers have been widely investigated for gas storage and separation, sensors, drug delivery, and catalysis, *etc.*, due to their large surface areas, high porosity, and easy structural and functional adjustment.[16–29] In recent years, through rational design or post-synthetic modification, functionalized MOFs have been endowed with potential applications in artificial photosynthesis.[30–37] However, most of those works focus on the reductive half-reaction but not the water oxidative half-reaction. As one of the important branches of MOFs, zeolitic imidazolate frameworks (ZIFs) are composed of metal ions and imidazole ligands.[38] Their structure and physical and chemical properties have many similarities with zeolite, such

as good thermal stability and chemical stability. Unfortunately, most of the ZIFs are constructed using metal ions with a tetrahedral coordination geometry that mimics the SiO_4 tetrahedral units in zeolites, resulting in only coordination-saturated metal centers within them. This is not beneficial for further applications in catalysis. The incorporation of unsaturated metal sites inside ZIFs is still challenging.[39–41]

In this work, we reported a solvent/atmosphere-assisted method to construct a new ZIF with coordinated unsaturated metal sites by manipulating the atmosphere and concentration of deprotonated solvent. The ZIF named **CoBIM-1**, constructed by 1,2-bis((5*H*-imidazol-4-yl)methylene)hydrazine (H_2BIM) ligand and cobalt(II) nitrate, was synthesized under low concentration of deprotonated solvent and inert atmosphere. As a control, **CoBIM-2** with coordination-saturated Co sites was also synthesized using a higher concentration of deprotonated solvent and an air atmosphere. Compared with **CoBIM-2**, **CoBIM-1** could efficiently photocatalyze water oxidation with $Ru(bpy)_3Cl_2$ (bpy, 2,2′-bipyridine) as the photosensitizer and $Na_2S_2O_8$ as the sacrificial electron acceptor in a borate buffer solution. An O_2 production of 2.0 mmol g^{-1} h^{-1} was observed in a borate buffer solution at pH of 8.4. Through isotope tracing experiments, it was confirmed that the produced dioxygen came from water oxidation.
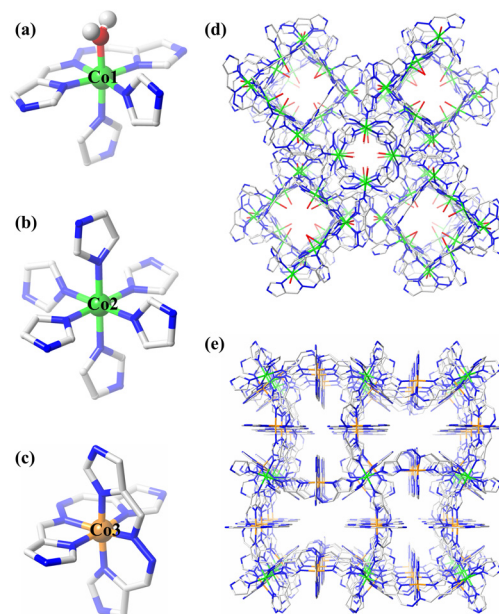

Fig. 1 Crystal structure of **CoBIM-1** and **CoBIM-2**. The coordination environment of cobalt ions in (a) **CoBIM-1** and (b, c) **CoBIM-2**, respectively. The three-dimensional structure of (d) **CoBIM-1** and (e) **CoBIM-2** along *a* axis, respectively. Colour codes: Co[II] green, Co[III] orange, N blue, O red, C grey, and H white.

Results and discussion

The reaction of the ligand BIM with cobalt(II) nitrate in a mixed solvent (DMF/methanol, 1/4, v/v) under a nitrogen atmosphere produces purple polyhedral crystals denoted as **CoBIM-1**. When the same ligand and metal salt are used but under an air atmosphere and with a higher concentration of DMF (DMF/methanol, 4/1, v/v), the reaction produces orange cubic crystals denoted as **CoBIM-2**. Single crystal X-ray diffraction (SCXRD) studies revealed that **CoBIM-1** crystallizes in space group $Ia\bar{3}d$, featuring a **gie** topology (Fig. 1d).[39] The coordination environment of the Co1 ion in **CoBIM-1** adopts an octahedral geometry, coordinating with 5 nitrogen atoms (from BIM) and 1 oxygen atom (from H_2O) (Fig. 1a). In contrast, **CoBIM-2** crystallizes in space group $Im\bar{3}$, featuring a **pcu** topology (Fig. 1e, S1, and S2†). There are two types of cobalt ion centers with different coordination environments in **CoBIM-2** (Fig. 1b and c). The Co2 ion adopts an octahedral geometry, coordinating with 6 nitrogen atoms from six imidazole parts of BIMs, while the Co3 ion adopts an octahedral geometry, coordinating with 6 nitrogen atoms from one BIM and one undeprotonated H_2BIM. The H_2BIM ligands are hung in the pores and do not participate in the expansion to form the three-dimensional structure (Fig. 1e).

The structural differences between **CoBIM-1** and **CoBIM-2** are reflected in the following two aspects: (1) different length of Co–N coordination bonds; (2) difference valence state of cobalt ions. In the **CoBIM-1**, the Co1–N bond distances are in the range of 1.918(5)–1.998(15) Å and the Co–O bond distance is 1.986(7) Å. In contrast, distances of all Co2–N bonds in

CoBIM-2 are 2.147(4) Å, while the Co3–N bond distances are in the range of 1.872(18)–1.914(8) Å. The obviously longer Co1–N bonds in **CoBIM-1** and Co2–N bonds in **CoBIM-2** than that of Co3–N bonds indicate that the Co1 and Co2 centers tend to have +2 oxidation states, while Co3 centers have +3 oxidation states.[42] Based on the above information and the results of elemental analysis, the chemical formulas of **CoBIM-1** and **CoBIM-2** are $[Co^{II}(BIM)(H_2O)]\cdot CH_3OH\cdot 4.5H_2O$ and $[Co^{III}_3Co^{II}(BIM)_3(H_2BIM)_3]\cdot 5NO_3\cdot 4CH_3OH$, respectively.

Thermogravimetric analysis (TGA) showed that **CoBIM-1** was stable up to around 250 °C (Fig. 2a). *In situ* variable temperature powder X-ray diffraction (PXRD) patterns further confirmed the high temperature tolerance of **CoBIM-1** (Fig. S5†). **CoBIM-1** was also quite stable in common organic solvents (*e.g.*, CH_3OH, CH_3CN) and water for one month at room temperature (Fig. S6†). Moreover, **CoBIM-1** showed good stability after being soaked in aqueous solutions over a wide pH range for one week (Fig. 2b). All of the above reflect that **CoBIM-1** has good thermal and chemical stability. In addition, the data from the TGA plot (Fig. S7†) and the PXRD patterns after being soaked in water for a week (Fig. S8†) also confirm that **CoBIM-2** has good thermal and hydrolytic stability.

To confirm the permanent porosity of **CoBIM-1** and **CoBIM-2**, N_2 adsorption/desorption isotherm measurements at 77 K were carried out. The N_2 adsorption isotherm of **CoBIM-1** showed a type-I isotherm for microporous materials (Fig. 2c). The BET and Langmuir surface areas of **CoBIM-1** were calculated to be 752 and 853 m² g^{-1}, respectively. The pore size distribution of **CoBIM-1** calculated by the DFT model showed that

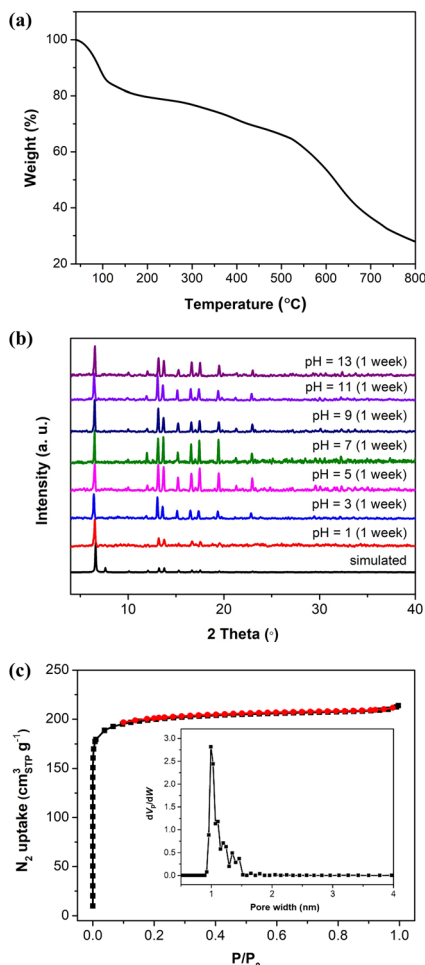This journal is © the Partner Organisations 2024

Inorg. Chem. Front., 2024, **11**, 5484–5489 | **5485**

Fig. 2 (a) TGA plot under a N_2 atmosphere of **CoBIM-1**. (b) PXRD patterns of **CoBIM-1** in H_2O with different pH for one week. (c) The N_2 adsorption (black dotted line) and desorption (red dotted line) isotherms at 77 K of **CoBIM-1**. The inset is the DFT pore size distributions.

its pores range from 9.9 to 14.5 Å (inset of Fig. 2c). Moreover, the water vapor adsorption isotherm of **CoBIM-1** at 298 K displayed a type-I characteristic and an uptake of 268 cm^3 g^{-1} (Fig. S9†), confirming the hydrophilic nature of internal pore surface.[41] Additionally, the porosity of **CoBIM-2** was confirmed by N_2 adsorption isotherm at 77 K (Fig. S10†), and its BET surface area was 66 m^2 g^{-1}. The reason for its small surface area may be that the H_2BIM ligands hung in the pore channels occupy most of the cavities.

In order to determine whether the coordinated unsaturated Co sites in Co-ZIF are beneficial for photocatalytic water oxidation reaction, both **CoBIM-1** and **CoBIM-2** are used as catalysts for evaluation. The solid-state UV-vis absorption spectrum showed that **CoBIM-1** had a broader light absorption range in the visible light area than that of **CoBIM-2** (Fig. S11†). Next, A 10.0 mL degassed borate buffer solution (pH = 8.2) containing 10 mg of **CoBIM-1** or **CoBIM-2**, 30.0 mM of $Na_2S_2O_8$, and 6.0 mM of $[Ru(bpy)_3]^{2+}$ (bpy = 2,2′-bipyridine) was irradiated using a 470 nm light-emitting diode (LED) lamp. The photoca-
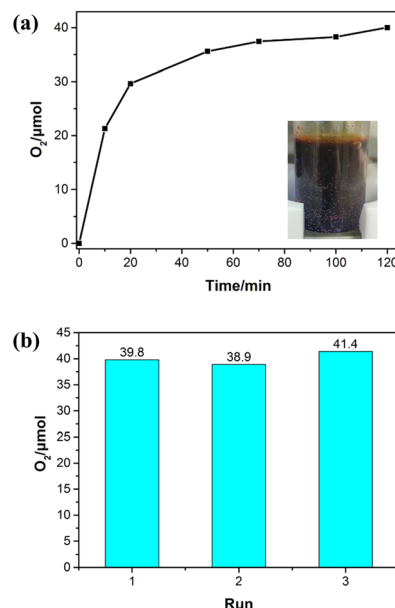

Fig. 3 (a) The time-dependent photocatalytic O_2 evolution and (b) recycling performance of **CoBIM-1**.

talytically produced O_2 was quantified using gas chromatography (GC). As shown in Fig. 3a, in the system with **CoBIM-1** as the catalyst, the generated O_2 increased with time and almost reached a plateau after two hours of reaction. Around 40.0 μmol of O_2 was generated with a production of 2.0 mmol g^{-1} h^{-1}. This O_2 production capacity is better than some reported MOF materials,[43] *e.g.*, $[Ru(tpy)(dcbpy)(OH_2)]^{2+}$ doped UiO-67 (0.04 mmol g^{-1} h^{-1}),[44] $[Bi(BTC)(DMF)]·DMF(CH_3OH)_2$ (0.8 mmol g^{-1} h^{-1}),[45] Bi-MOF (1.1 mmol g^{-1} h^{-1}),[46] Cd-TBAPy (1.6 mmol g^{-1} h^{-1}),[47] *etc.* Moreover, based on the amount of $Na_2S_2O_8$ used, the yield of O_2 in this system was calculated to be 26.7%. No O_2 evolution was observed without $Ru(bpy)_3Cl_2$, $Na_2S_2O_8$, or **CoBIM-1** during the photocatalytic process (Table 1). The control experiments indicated that **CoBIM-1** was indeed active towards water oxidation reaction. To prove that the O_2 was produced by water oxidation, an isotope-labelling water oxidation experiment was performed with **CoBIM-1** as the photocatalyst and $H_2^{18}O$ as the solvent. As shown in Fig. S12,† $^{18}O_2$ was detected, confirming the above conclusion.

Table 1 The amount of O_2 evolution of **CoBIM-1** and **CoBIM-2** as photocatalysts, respectively

Catalysts	$Ru(bpy)_3Cl_2$ (mM)	$Na_2S_2O_8$ (mM)	O_2 (μmol)
CoBIM-1	—	30	None
CoBIM-1	6	—	None
—	6	30	None
CoBIM-1	6	30	40.0
CoBIM-2	6	30	None

Conditions: degassed borate buffer solution, 10.0 mL; catalysts, 10 mg; reaction time, 2 h; pH, 8.2; light source, 470 nm LED.

5486 | *Inorg. Chem. Front.*, 2024, **11**, 5484–5489

This journal is © the Partner Organisations 2024

Notably, **CoBIM-2** showed no activity towards water oxidation due to the lack of coordinatively unsaturated Co sites.

The cyclic catalytic testing of **CoBIM-1** showed that its catalytic activity could be well maintained after at least three runs (Fig. 3b and S13†). The retained PXRD pattern further indicated that the crystal structure remained intact after three rounds of the photocatalytic process (Fig. S14†). We also found the size of **CoBIM-1** can influence the catalytic performance and the smaller crystals are benefit for the catalytic activity toward water oxidation (Fig. S15, S16 and Table S2†). It may be that the smaller size of **CoBIM-1** is more conducive to the exposure of catalytic sites.

Based on the above experimental results, **CoBIM-1** can indeed decompose H_2O into O_2 in the $[Ru(bpy)_3]^{2+}$-$Na_2S_2O_8$ system with visible light irradiation. According to previous reports on the mechanism of the photocatalyzed water oxidation reaction using cobalt-containing MOF catalysts,[48] we speculate the possible mechanism of the photocatalytic water oxidation reaction of **CoBIM-1** as follows. (1) The photosensitizer $[Ru(bpy)_3]^{2+}$ is excited by visible light to form $[Ru(bpy)_3]^{2+*}$ (* represents an excited state). (2) After transferring electrons to $S_2O_8^{2-}$, the active $[Ru(bpy)_3]^{2+*}$ is oxidized to $[Ru(bpy)_3]^{3+}$. The sacrificial agent $S_2O_8^{2-}$ is reduced to SO_4^{2-} and $SO_4^{\bullet-}$ radicals as well. (3) The electrode potential of the $SO_4^{\bullet-}$ radical is higher than the electrode potential of $[Ru(bpy)_3]^{2+}/[Ru(bpy)_3]^{3+}$. As a result, two molecules of $SO_4^{\bullet-}$ radical can oxidize $[Ru(bpy)_3]^{2+}$ to $[Ru(bpy)_3]^{3+}$. (4) $[Ru(bpy)_3]^{3+}$ can accept electrons from **CoBIM-1** and is reduced to $[Ru(bpy)_3]^{2+}$. The oxidized **CoBIM-1** can then catalyze the water oxidation reaction to produce O_2.

Conclusions

In summary, we have synthesized two new Co-ZIFs (**CoBIM-1** and **CoBIM-2**) using the same cobalt salt and BIM ligand. The coordination-unsaturated Co sites inside Co-ZIF can be achieved by manipulating the atmosphere and concentration of deprotonated solvent during the synthesis process. Under reaction conditions of a high concentration of deprotonated solvent and an inert atmosphere, **CoBIM-1** with coordination-unsaturated Co sites was obtained. In contrast, the case of **CoBIM-2** with coordination-saturated Co sites was obtained under a lower concentration of deprotonated solvent and an air atmosphere. Both **CoBIM-1** and **CoBIM-2** exhibited good chemical and thermal stability. Compared with **CoBIM-2**, **CoBIM-1**, with coordination-unsaturated Co sites, exhibited good performance in photocatalytic water oxidation with an O_2 production of 2.0 mmol g^{-1} h^{-1} under 470 nm light irradiation. Besides, **CoBIM-1** also showed good recyclability. The isotope-labelling water oxidation experiment further proved that O_2 was produced by the photocatalytic water oxidation reaction. This work provides an interesting method for synthesizing MOF materials with coordination-unsaturated metal sites and applying them to photocatalytic water oxidation, which is inspiring for the synthesis of similar photocatalysts for water splitting.

Experimental

Synthesis of CoBIM-1

In a nitrogen atmosphere, the reaction of ligand BIM (0.03 mmol) with cobalt(II) nitrate hexahydrate (0.03 mmol) in a mixed solvent (DMF/methanol, 1/4, v/v) under solvothermal conditions (110 °C, 72 h) afforded purple polyhedral crystals denoted as **CoBIM-1**. In order to obtain high yields of samples, degassing conditions are necessary. The samples were soaked in methanol for solvent exchange, and fresh methanol was replaced every day for three days. The solid sample was collected by filtration. Elemental analysis (CHN), $CoC_9H_{21}N_6O_{6.5}$ (corresponding to $[Co^{II}(BIM)(H_2O)]\cdot CH_3OH\cdot 4.5H_2O$), calculated (%): C, 28.73; H, 5.63; N, 22.34. Found (%): C, 28.60; H, 4.48; N, 22.34.

Smaller purple polyhedral crystals of **CoBIM-1**, all less than 10 μm in size, were obtained by the following method. The entire mixture, including BIM (0.06 mmol), cobalt(II) nitrate hexahydrate (0.06 mmol), and DMF/methanol solvent (1/4, v/v), was reacted under stirring (200 rpm) with a magnetic bar for 24 hours. Additionally, samples with a size of about 5 μm could be produced by increasing the stirring speed to 400 rpm. Lastly, nanoscaled **CoBIM-1** was obtained by grinding the sample in a ball mill with a rotation speed of 1200 rpm.

Synthesis of CoBIM-2

The ligand BIM (0.03 mmol) was reacted with cobalt(II) nitrate hexahydrate (0.02 mmol) in a mixed solvent (DMF/methanol, 4/1, v/v) under solvothermal conditions (110 °C, 72 h), resulting in the formation of orange cubic crystals as a product (denoted as **CoBIM-2**). The samples were soaked in methanol for solvent exchange, and fresh methanol was replaced every day for three days. The solid sample was collected by filtration. Elemental analysis (CHN), $Co_4C_{52}H_{58}N_{41}O_{19}$ (corresponding to $[Co^{III}_3Co^{II}(BIM)_3(H_2BIM)_3]\cdot 5NO_3\cdot 4CH_3OH$), calculated (%): C, 34.76; H, 3.25; N, 31.96. Found (%): C, 37.49; H, 3.24; N, 32.37.

Photocatalytic water oxidation experiments

The photocatalytic water oxidation experiments were conducted in a quartz tube using the WP-TEC-1020H system. Specifically, **CoBIM-1** or **CoBIM-2**, $Ru(bpy)_3Cl_2$, and $Na_2S_2O_8$ were added to the quartz tube along with 10 mL of degassed borate buffer solution (pH = 8.2). The mixture in the tube was then bubbled with argon for half an hour before starting the reaction by turning on the LED lamp. The generated gas was analysed by gas chromatography (GC9790II) with a TCD detector.

Data availability

The data supporting this article have been included as part of the ESI.†

This journal is © the Partner Organisations 2024

Inorg. Chem. Front., 2024, **11**, 5484–5489 | **5487**

Conflicts of interest

There are no conflicts to declare.

Acknowledgements

References

1 Z. Wang, Y. Hu, S. Zhang and Y. Sun, Artificial photosynthesis systems for solar energy conversion and storage: platforms and their realities, *Chem. Soc. Rev.*, 2022, **51**, 6704–6737.

2 B. Zhang and L. Sun, Artificial photosynthesis: opportunities and challenges of molecular catalysts, *Chem. Soc. Rev.*, 2019, **48**, 2216–2264.

3 J. Lv, J. Xie, A. G. A. Mohamed, X. Zhang, Y. Feng, L. Jiao, E. Zhou, D. Yuan and Y. Wang, Solar utilization beyond photosynthesis, *Nat. Rev. Chem.*, 2023, **7**, 91–105.

4 W. Zhang and R. Cao, Water oxidation with polymeric photocatalysts, *Chem. Rev.*, 2022, **122**, 5408–5410.

5 Y. Kurashige, G. K. Chan and T. Yanai, Entangled quantum electronic wavefunctions of the Mn_4CaO_5 cluster in photosystem II, *Nat. Chem.*, 2013, **5**, 660–666.

6 C. J. Kim and R. J. Debus, One of the substrate waters for O_2 formation in photosystem II is provided by the water-splitting Mn_4CaO_5 cluster's Ca^{2+} ion, *Biochemistry*, 2019, **58**, 3185–3192.

7 H. Tamura, K. Saito, S. Nishio and H. Ishikita, Electron-transfer route in the early oxidation states of the Mn_4CaO_5 cluster in photosystem II, *J. Phys. Chem. B*, 2023, **127**, 205–211.

8 J. M. Gonçalves, M. Ireno da Silva, L. Angnes and K. Araki, Vanadium-containing electro and photocatalysts for the oxygen evolution reaction: a review, *J. Mater. Chem. A*, 2020, **8**, 2171–2206.

9 H. Ye, Z. Wang, K. Hu, W. Wu, X. Gong and J. Hua, FeOOH photo-deposited perylene linear polymer with accelerated charge separation for photocatalytic overall water splitting, *Sci. China: Chem.*, 2022, **65**, 170–181.

10 C.-F. Fu, C. Zhao, Q. Zheng, X. Li, J. Zhao and J. Yang, Halogen modified two-dimensional covalent triazine frameworks as visible-light driven photocatalysts for overall water splitting, *Sci. China: Chem.*, 2020, **63**, 1134–1141.

11 V. Artero, M. Chavarot-Kerlidou and M. Fontecave, Splitting water with cobalt, *Angew. Chem., Int. Ed.*, 2011, **50**, 7238–7266.

12 H. S. Ahn and T. D. Tilley, Electrocatalytic water oxidation at neutral pH by a nanostructured $Co(PO_3)_2$ anode, *Adv. Funct. Mater.*, 2013, **23**, 227–233.

13 N. S. McCool, D. M. Robinson, J. E. Sheats and G. C. Dismukes, A Co_4O_4 "cubane" water oxidation catalyst inspired by photosynthesis, *J. Am. Chem. Soc.*, 2011, **133**, 11446–11449.

14 M. Zhang, M. de Respinis and H. Frei, Time-resolved observations of water oxidation intermediates on a cobalt oxide nanoparticle catalyst, *Nat. Chem.*, 2014, **6**, 362–367.

15 Z. Y. Chen, Z. H. Long, X. Z. Wang, J. Y. Zhou, X. S. Wang, X. P. Zhou and D. Li, Cobalt-based metal-organic cages for visible-light-driven water oxidation, *Inorg. Chem.*, 2021, **60**, 10380–10386.

16 Y. Peng, S. Sanati, A. Morsali and H. García, Metal–organic frameworks as electrocatalysts, *Angew. Chem., Int. Ed.*, 2023, **62**, e202214707.

17 X. Li, G. Jiang, M. Jian, C. Zhao, J. Hou, A. W. Thornton, X. Zhang, J. Z. Liu, B. D. Freeman, H. Wang, L. Jiang and H. Zhang, Construction of angstrom-scale ion channels with versatile pore configurations and sizes by metal-organic frameworks, *Nat. Commun.*, 2023, **14**, 286.

18 X. Zhang, J. Maddock, T. M. Nenoff, M. A. Denecke, S. Yang and M. Schroder, Adsorption of iodine in metal-organic framework materials, *Chem. Soc. Rev.*, 2022, **51**, 3243–3262.

19 Y. Zhang, K. Ren, L. Wang, L. Wang and Z. Fan, Porphyrin-based heterogeneous photocatalysts for solar energy conversion, *Chin. Chem. Lett.*, 2022, **33**, 33–60.

20 F. Mua, B. Daia, W. Zhao, L. Zhang, J. Xu and X. Guo, A review on metal-organic frameworks for photoelectrocatalytic applications, *Chin. Chem. Lett.*, 2020, **31**, 1773–1781.

21 N. Hu, Y. Cai, L. Li, X. Wang and J. Gao, Amino-functionalized titanium based metal-organic framework for photocatalytic hydrogen production, *Molecules*, 2022, **27**, 4241.

22 X. Wang, X. Yang, C. Chen, H. Li, Y. Huang and R. Cao, Graphene quantum dots supported on Fe-based metal-organic frameworks for efficient photocatalytic CO_2 reduction, *Acta Chim. Sin.*, 2022, **80**, 22–28.

23 Y. B. Huang, J. Liang, X. S. Wang and R. Cao, Multifunctional metal-organic framework catalysts: synergistic catalysis and tandem reactions, *Chem. Soc. Rev.*, 2017, **46**, 126–157.

24 R.-J. Wei, H.-G. Zhou, Z.-Y. Zhang, G.-H. Ning and D. Li, Copper(I)–organic frameworks for catalysis: networking metal clusters with dynamic covalent chemistry, *CCS Chem.*, 2021, **3**, 2045–2053.

25 Y. Xiao, X. Guo, T. Yang, J. Liu, X. Liu, Y. Xiao, L. Liu, T. Liu, S. Ye, J. Jiang, F. Zhang and C. Li, Water-stable Mn-based MOF nanosheet as robust visible-light-responsive photocatalyst in aqueous solution, *Sci. China: Chem.*, 2020, **63**, 1756–1760.

5488 | *Inorg. Chem. Front.*, 2024, **11**, 5484–5489

This journal is © the Partner Organisations 2024

26 Q. Zuo, R. Cui, L. Wang, Y. Wang, C. Yu, L. Wu, Y. Mai and Y. Zhou, High-loading single cobalt atoms on ultrathin MOF nanosheets for efficient photocatalytic CO$_2$ reduction, *Sci. China: Chem.*, 2023, **66**, 570–577.

27 S. Wang, Y. Hou, S. Lin and X. Wang, Water oxidation electrocatalysis by a zeolitic imidazolate framework, *Nanoscale*, 2014, **6**, 9930–9934.

28 S. Wang and X. Wang, *Small*, 2015, **11**, 3097–3112.

29 J. Chen, B. An, Y. Chen, X. Han, Q. Mei, M. He, Y. Cheng, I. J. Vitorica-Yrezabal, L. S. Natrajan, D. Lee, A. J. Ramirez-Cuesta, S. Yang and M. Schröder, *J. Am. Chem. Soc.*, 2023, **145**, 19225–19231.

30 Q. Yu, X. Wang, W. Wu, X. Feng, D. Kong, U. Khan, X. Ren and L. Li, In situ encapsulation of graphene quantum dots in highly stable porphyrin metal-organic frameworks for efficient photocatalytic CO$_2$ reduction, *Molecules*, 2023, **28**, 4703.

31 H. Zhang, Q. Li, B. Weng, L. Xiao, Z. Tian, J. Yang, T. Liu and F. Lai, Edge engineering of platinum nanoparticles via porphyrin-based ultrathin 2D metal–organic frameworks for enhanced photocatalytic hydrogen generation, *Chem. Eng. J.*, 2022, **442**, 136144.

32 X. S. Wang, L. Li, D. Li and J. Ye, Recent progress on exploring stable metal–organic frameworks for photocatalytic solar fuel production, *Sol. RRL*, 2020, **4**, 1900547.

33 H. Hu, Z. Wang, L. Cao, L. Zeng, C. Zhang, W. Lin and C. Wang, Metal-organic frameworks embedded in a liposome facilitate overall photocatalytic water splitting, *Nat. Chem.*, 2021, **13**, 358–366.

34 S. Zhang, G. Cheng, L. Guo, N. Wang, B. Tan and S. Jin, Strong base assisted synthesis of crystalline covalent triazine framework with high hydrophilicity via benzylamine monomer for photocatalytic water splitting, *Angew. Chem., Int. Ed.*, 2020, **59**, 6007–6014.

35 T. Takata, J. Jiang, Y. Sakata, M. Nakabayashi, N. Shibata, V. Nandal, K. Seki, T. Hisatomi and K. Domen, Photocatalytic water splitting with a quantum efficiency of almost unity, *Nature*, 2020, **581**, 411–414.

36 E. X. Chen, M. Qiu, Y. F. Zhang, L. He, Y. Y. Sun, H. L. Zheng, X. Wu, J. Zhang and Q. Lin, Energy band alignment and redox-active sites in metalloporphyrin-spaced metal-catechol frameworks for enhanced CO$_2$ photoreduction, *Angew. Chem., Int. Ed.*, 2022, **61**, e202111622.

37 Z. Jiang, X. Xu, Y. Ma, H. S. Cho, D. Ding, C. Wang, J. Wu, P. Oleynikov, M. Jia, J. Cheng, Y. Zhou, O. Terasaki, T. Peng, L. Zan and H. Deng, Filling metal-organic framework mesopores with TiO$_2$ for CO$_2$ photoreduction, *Nature*, 2020, **586**, 549–554.

38 H. Hayashi, A. P. Cote, H. Furukawa, M. O'Keeffe and O. M. Yaghi, Zeolite A imidazolate frameworks, *Nat. Mater.*, 2007, **6**, 501–506.

39 X. P. Zhou, M. Li, J. Liu and D. Li, Gyroidal metal-organic frameworks, *J. Am. Chem. Soc.*, 2012, **134**, 67–70.

40 Y. Wu, X. P. Zhou, J. R. Yang and D. Li, Gyroidal metal-organic frameworks by solvothermal subcomponent self-assembly, *Chem. Commun.*, 2013, **49**, 3413–3415.

41 D. Luo, Y.-L. Peng, M. Xie, M. Li, A. A. Bezrukov, T. Zuo, X.-Z. Wang, Y. Wu, Y. Y. Li, A. R. Lowe, M. Chorążewski, Y. Grosu, Z. Zhang, M. J. Zaworotko, X.-P. Zhou and D. Li, Improving Ethane/Ethylene Separation Performance under Humid Conditions by Spatially Modified Zeolitic Imidazolate Frameworks, *ACS Appl. Mater. Interfaces*, 2022, **14**, 11547–11558.

42 L. Liang, D. Luo, T. Zuo, X.-P. Zhou and D. Li, Control over the synthesis of homovalent and mixed-valence cubic cobalt-imidazolate cages, *Chem. Commun.*, 2019, **55**, 5103–5106.

43 S. Navalón, A. Dhakshinamoorthy, M. Alvaro, B. Ferrer and H. García, Metal−Organic Frameworks as Photocatalysts for Solar-Driven Overall Water Splitting, *Chem. Rev.*, 2023, **123**, 445–490.

44 S. Lin, A. Ravari, J. M. Zhu, P. M. Usov, M. Cai, S. R. Ahrenholtz, Y. Pushkar and A. J. Morris, Insight into MetalOrganic Framework Reactivity: Chemical Water Oxidation Catalyzed by a $[Ru(tpy)(dcbpy)(OH_2)]^{2+}$-Modified UiO-67, *ChemSusChem*, 2018, **11**, 464–471.

45 G. Wang, Y. Liu, B. Huang, X. Qin, X. Zhang and Y. Dai, A Novel Metal-Organic Framework Based on Bismuth and Trimesic Acid: Synthesis, Structure and Properties, *Dalton Trans.*, 2015, **44**, 16238–16241.

46 Y. Liu, G. Wang, J. Dong, Y. An, B. Huang, X. Qin, X. Zhang and Y. Dai, A Bismuth based Layer Structured Organic-Inorganic Hybrid Material with Enhanced Photocatalytic Activity, *J. Colloid Interface Sci.*, 2016, **469**, 231–236.

47 Y. Xiao, Y. Qi, X. Wang, X. Wang, F. Zhang and C. Li, VisibleLight-Responsive 2D Cadmium-Organic Framework Single Crystals with Dual Functions of Water Reduction and Oxidation, *Adv. Mater.*, 2018, **30**, 1803401.

48 G. Paille, M. Gomez-Mingot, C. Roch-Marchal, B. Lassalle-Kaiser, P. Mialane, M. Fontecave, C. Mellot-Draznieks and A. Dolbecq, A fully noble metal-free photosystem based on cobalt-polyoxometalates immobilized in a porphyrinic metal-organic framework for water oxidation, *J. Am. Chem. Soc.*, 2018, **140**, 3613–3618.

This journal is © the Partner Organisations 2024

Inorg. Chem. Front., 2024, **11**, 5484–5489 | **5489**